Eur. Phys. J. B (2017) 90: 33
DOI: 10.1140/epjb/e2017-70705-8

THE EUROPEAN PHYSICAL JOURNAL B

Regular Article

Tunneling conductance study of a metal-superconductor junction in the presence of Rashba spin orbit coupling

Priyadarshini Kapri[a] and Saurabh Basu

Department of Physics, Indian Institute of Technology Guwahati, 781039 Assam, India

Received 25 November 2016 / Received in final form 10 January 2017
Published online 13 February 2017 –

Abstract. The tunneling conductance for a junction device consisting of a normal metal and a singlet superconductor is studied with Rashba spin orbit coupling (RSOC) being present in the metallic lead and the interface separating the two regions via an extended Blonder-Tinkham-Klapwijk (BTK) formalism. Interesting interplay between the RSOC and a number of parameters that have experimental significance, and characterize either the junction or the superconducting leads, such as the barrier transparency, quasiparticle lifetime, Fermi wavevector mismatch, an in-plane magnetic field and their effects on the tunneling conductance are investigated in details for both a *s*-wave and a *d*-wave superconductor. In an opaque barrier, in presence of a quasiparticle lifetime, a Fermi wavevector mismatch or an external in-plane magnetic field, RSOC enhances the conductance corresponding to low biasing energies, that is, at energies lesser than the superconducting gap, while the reverse is noted for energies exceeding the magnitude of the gap. Further, there are exciting anomalies noted in the conductance spectrum for the *d*-wave gap which can be understood by incorporating the interplay between the superconducting gap and the angle of incident of the charge carriers.

1 Introduction

Studies of electron transport through normal metal – superconductor (N-S) junctions have proved to have a great deal of interest owing to the fundamental physics embedded therein and the possibility of fabricating devices. Tunneling spectroscopy at a N-S junction is one of the most effective tool to investigate the nature of the superconducting state [1,2]. The fundamental physics includes probing of the electronic states in the normal metal and thereby acquiring information on the interparticle interaction and the nature of the superconducting gap. The low energy transmission characteristics are dominated by the Andreev reflection (AR) [3–5] caused by the conversion of current in the normal region to a supercurrent in the superconductor at the N-S junction. The ramifications of AR is in the enhancement of conductance of a N-S junction device beyond its normal state value in the sub-gap region. The Blonder-Tinkham-Klapwijk (BTK) theory [6] provides a simple description of the AR by modeling the N-S interface via a δ- function potential (or an insulating barrier of arbitrary strength) where the quasiparticle propagation in the superconducting sample is described by the Bogoliubov-de Gennes (BdG) equations [7] and the wavefunctions are matched with the normal state wavefunctions at the interface.

With the advent of spintronics in the recent past, the ability to manipulate the spin degree of freedom with precision, just like the charge degree of freedom has gained prominence. The phenomenon of spin-orbit coupling (SOC) is central to the process of this emerging field. In low dimensions, particularly, in the context of two dimensional electron gases (2DEG), a system where the surface inversion symmetry is lost, such as InAs etc. [8], a special type of SOC, that is, Rashba spin-orbit coupling [9] becomes important and hence can not be neglected. The possibility of being able to tune the strength of Rashba SOC (RSOC) using an external field [10] provides additional impetus. A few studies have been carried out to understand the effect of RSOC in N-S interface [11–13].

Motivated by the above, we employ a BTK formalism to perform an extensive investigation of the conductance characteristics of a normal metal-singlet superconductor (both *s*-wave and *d*-wave) junction in the presence of RSOC with the Rashba term being present in the metallic lead and the interface. We are particularly interested in examining an interplay of RSOC with a number of useful parameters that are indispensable in a N-S junction device. These parameters include transparency of the N-S interface, finite quasiparticle lifetime, Fermi wavevector mismatch between the carriers in the metallic region with that of the quasiparticles in the superconductor and an in-plane magnetic field present in the system. We shall mention the experimental relevance and hence the importance of these

[a] e-mail: priyadarshini@iitg.ernet.in

parameters as we go along discussing the key results of our paper.

A holistic view towards the work at hand reveals that the conductance properties of a N-S junction device can be manipulated by the RSOC present in the metallic lead and the boundary separating the normal and the superconducting region. Further the interplay between the RSOC and a few of the physical quantities, that are essentially properties of the interface or the superconducting leads, renormalize the features of the low energy conductance spectrum.

While both s-wave and d-wave denote singlet superconducting pairing correlations, we emphasize that there is a distinction in the conductance profile with regard to the interplay between the RSOC and the various parameters that are mentioned above. Thus the symmetry of the superconducting gap plays a decisive role in the conductance properties of a N-S junction.

We provide a brief outline of the BTK formalism in the next section for completeness of our discussion and establishing the notations that are used throughout the paper. The results and their corresponding discussions follow afterwards. Finally we conclude with a mention of the highlights of our work.

2 Conductance formula: BTK model

We consider a two dimensional N-S junction as shown in Figure 1a where an interface is located at $x = 0$, the left of which being a normal metal (N) with a superconducting (S) lead in the right. The interaction potential everywhere is described by,

$$U_\sigma(x) = U\hat{n}\cdot(\hat{\sigma}\times\hat{k})\Theta(-x) + (U_0 + U\hat{n}\cdot(\hat{\sigma}\times\hat{k}))\delta_{x,0} \quad (1)$$

where $\hat{n} = \hat{x}$ is the unit vector along the interface normal, U_0 is the strength of spin independent potential barrier at the interface, U is the strength of the RSOC for N region and interfacial region (U has the dimension of energy scaled by the Fermi wavevector for the normal metal, k_{FN}), $\hat{\sigma}$ are the Pauli matrices, $\hat{k} = -i\nabla$ ($\hbar = 1$) and $\Theta(x)$ is the Heaviside function.

The Bogoliubov de Gennes (BdG) equations [7] are used here to describe the quasiparticles. The quasiparticle wave function has four components because of the extra spin degrees of freedom due to the Rashba term. By considering a two dimensional geometry, the BdG equations can be decoupled into two component equations, one for each spin, σ, as follows,

$$H_\sigma\Psi(r) = E\Psi(r) \quad (2)$$

where $\sigma = \pm 1$ denote two different spin orientations. H_σ is written as,

$$H_\sigma = \begin{pmatrix} -\frac{\nabla^2}{2} - E_{Fi} + U_\sigma(x) & \tilde{\Delta} \\ \tilde{\Delta}^\dagger & \frac{\nabla^2}{2} + E_{Fi} - U_\sigma(x) \end{pmatrix} \quad (3)$$

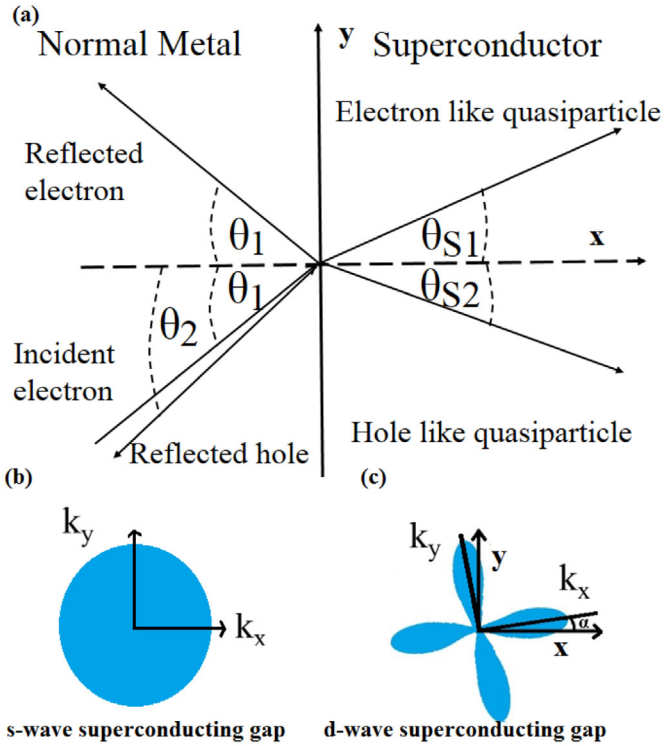

Fig. 1. (a) Schematic illustration of the reflection and the transmission process of the quasiparticle at N-S junction. (b) Profile for s-wave superconducting gap. (c) Profile for d-wave superconducting gap.

where the electronic mass is taken as unity. The interaction term can explicitly be written as,

$$U_\sigma(x) = (U_0 - \sigma U k_{FN}\sin\theta_1)\delta_{x,0} - \sigma U k_{FN}\sin\theta_1\Theta(-x). \quad (4)$$

The Fermi energies in the normal region and the superconducting region are E_{FN} and E_{FS} respectively. The ratio of the corresponding wave vectors is denoted by the dimensionless parameter λ where $\lambda = q_{FS}/k_{FN} = \sqrt{E_{FS}/E_{FN}}$. The off-diagonal terms of the matrix are the superconducting gap parameter, $\tilde{\Delta}$. The superconducting order parameter for s-wave is given by,

$$\tilde{\Delta} = \Delta_0\Theta(x) \quad (5)$$

and the corresponding quantity for d-wave is

$$\tilde{\Delta} = \tilde{\Delta}_\pm = \Delta(k_\pm)\Theta(x) = \Delta_0\cos(2\theta_{S1,2} \mp 2\alpha)\Theta(x) \quad (6)$$

where α is the angle between the crystalline orientation and x axis as shown in Figure 1c, Δ_+ and Δ_- are the gap functions of electron and hole-like quasiparticles. The k dependence in the $\tilde{\Delta}_\pm$ enters through θ_{S1} and θ_{S2} (see Eq. (9)) and $\tilde{\Delta}$ has the dimension of energy. We note that the superconducting order parameter can be different for electron-like and hole-like quasiparticles.

To make our discussion clear, we refer to Figure 1a. Suppose an electron from the left metallic lead is injected with the excitation energy $E \geq 0$, spin σ, and incident angle θ_1, the incident electron will be reflected back either

as an electron (normal reflection) or as a hole (Andreev reflected hole). The momenta of electrons and holes in the normal region are given by k^+ and k^-,

$$k^+ = k_{FN} + \frac{\sigma U k_{FN}\sin\theta_1 + E}{v_{FN}}$$
$$k^- = k_{FN} + \frac{\sigma U k_{FN}\sin\theta_1 - E}{v_{FN}}. \quad (7)$$

Further the momenta of the electron-like and hole-like quasiparticles in superconducting region are given by q^+ and q^- which are,

$$q^+ = q_{FS} + \frac{\sqrt{E^2 - \tilde{\Delta_+}^2}}{v_{FS}}$$
$$q^- = q_{FS} - \frac{\sqrt{E^2 - \tilde{\Delta_-}^2}}{v_{FS}} \quad (8)$$

where v_{FN} and v_{FS} are Fermi velocities for respective regions. Please see Appendix A for derivation. Here we consider a simplification by setting $q^+ = q^- = q_{FS}$. This simplification introduces an error of the order $\delta q_{FS}/q_{FS} = \sqrt{E^2 - \tilde{\Delta}^2}/E_{FS}$, which is of the order $\tilde{\Delta}/E_{FS}$. Since $\tilde{\Delta}$ is much smaller than E_{FS}, this is a reasonable assumption. However we retain different symbols for them for the sake of completeness. The momentum parallel to the interface is conserved in the tunneling process. So we can write,

$$k^+\sin\theta_1 = k^-\sin\theta_2 = q^+\sin\theta_{S1} = q^-\sin\theta_{S2} \quad (9)$$

where θ_2 is angle of reflection of the hole due to AR, θ_{S1} and θ_{S2} are the angles of refraction of electron-like and hole-like quasiparticles respectively.

The solutions of equation (2) in normal metal and superconducting regions are found to be,

$$\Psi_N(x) = \begin{pmatrix}1\\0\end{pmatrix} e^{ik^+\cos\theta_1 x} + a_\sigma \begin{pmatrix}0\\1\end{pmatrix} e^{ik^-\cos\theta_2 x} + b_\sigma \begin{pmatrix}1\\0\end{pmatrix} e^{-ik^+\cos\theta_1 x} \quad (10)$$

and

$$\Psi_S(x) = c_\sigma \begin{pmatrix}u_+ e^{i\phi_+}\\ v_+\end{pmatrix} e^{iq^+\cos\theta_{S1}x} + d_\sigma \begin{pmatrix}v_- e^{i\phi_-}\\ u_-\end{pmatrix} e^{-iq^-\cos\theta_{S2}x} \quad (11)$$

respectively. Here a_σ and b_σ denote the amplitudes of Andreev reflection (AR) and normal reflection (NR) respectively. Also c_σ and d_σ correspond to coefficients of transmission to the superconductor leads as electron-like quasiparticles and as hole-like quasiparticles whose amplitudes are given by,

$$u_\pm = \frac{1}{\sqrt{2}}\sqrt{1 + \frac{\Omega_\pm}{E}}$$
$$v_\pm = \frac{1}{\sqrt{2}}\sqrt{1 - \frac{\Omega_\pm}{E}} \quad (12)$$

where

$$\Omega_\pm = \sqrt{E^2 - \tilde{\Delta}_\pm^2}. \quad (13)$$

The wave functions must satisfy the boundary conditions,

$$\Psi_S(x=0^+) = \Psi_N(x=0^-)$$
$$\frac{d\Psi_S}{dx}(x=0^+) - \frac{d\Psi_N}{dx}(x=0^-) = 2(U_0 - \sigma U k_{FN}\sin\theta_1)\Psi_N(x=0^-) \quad (14)$$

All the reflection and transmission amplitudes can be found from the boundary conditions.

In particular, for the reflection amplitudes we obtain,

$$a_\sigma(E,\theta_1) = \frac{Q\omega_-(P_1 - P_2)}{P_2P_3\omega_+\omega_- e^{i\phi_+} - P_1P_4 e^{i\phi_-}} \quad (15)$$

and

$$b_\sigma(E,\theta_1) = -Q\omega_+\omega_- \frac{P_2 e^{i\phi_+}}{P_2P_3\omega_+\omega_- e^{i\phi_+} - P_1P_4 e^{i\phi_-}} + \frac{QP_1 e^{i\phi_-}}{P_2P_3\omega_+\omega_- e^{i\phi_+} - P_1P_4 e^{i\phi_-}} - 1 \quad (16)$$

where,

$$Q = 2ik^+\cos\theta_1$$
$$\omega_\pm = \frac{u_\pm}{v_\pm}$$
$$e^{i\phi_\pm} = \tilde{\Delta_\pm}/|\tilde{\Delta_\pm}|. \quad (17)$$

The P_i's appearing above are denoted by,

$$P_1 = 2U_0 - 2\sigma U k_{FN}\sin\theta_1 + ik^-\cos\theta_2 - iq^+\cos\theta_{S1}$$
$$P_2 = 2U_0 - 2\sigma U k_{FN}\sin\theta_1 + ik^-\cos\theta_2 + iq^-\cos\theta_{S2}$$
$$P_3 = 2U_0 - 2\sigma U k_{FN}\sin\theta_1 - ik^+\cos\theta_1 - iq^+\cos\theta_{S1}$$
$$P_4 = 2U_0 - 2\sigma U k_{FN}\sin\theta_1 - ik^+\cos\theta_1 + iq^-\cos\theta_{S2}. \quad (18)$$

Using the BTK formalism, the normalized differential tunneling conductance at zero temperature is given by,

$$G(E) = \frac{G_S(E)}{G_N} \quad (19)$$

where we have

$$G_S(E) = \sum_\sigma \int_{-\pi/2}^{\pi/2} d\theta_1 \cos\theta_1 G_\sigma(E,\theta_1) \quad (20)$$

with the angle and spin resolved conductance $G_\sigma(E,\theta_1)$ is given by,

$$G_\sigma(E,\theta_1) = 1 + |a_\sigma(E,\theta_1)|^2\frac{k^-}{k^+} - |b_\sigma(E,\theta_1)|^2 \quad (21)$$

and

$$G_N = \sum_\sigma \int_{-\pi/2}^{\pi/2} d\theta_1 \cos\theta_1 \frac{4}{4 + Z_0^2/\cos\theta_1^2} \quad (22)$$

is the conductance for a normal metal-normal metal junction with a scaled interface potential, U_0, where $Z_0 = 2U_0/k_{FN}$. The consideration of different Fermi energies corresponding to two different regions imposes a further constraint on the effective range of angle contributing to the integral appearing in equation (20). As q_{FS} is made larger, the range of the angle θ_1 decreases as is evident from equation (9).

3 Rashba spin orbit coupling (RSOC)

In all our results presented below, we plot G as appears in equation (19) as a function of biasing energy, E scaled by the magnitude of the gap amplitude, Δ_0. It can be noted that the magnitude of the barrier strength at the interface will decide whether RSOC will enhance or decrease the value of the low energy conductance [14].

In Figure 2a, G is shown as function of E/Δ_0 for a s-wave superconductor as the strength of RSOC is varied corresponding to a transparent barrier, that is, $Z_0 = 0$. A dip in the AR peak is noted as RSOC is increased from $U = 1$ to $U = 2$. The Rashba free case ($U = 0$) is included for comparison. Apart from the decrease in peak conductance, a significant suppression of the low energy conductance is also noted.

For an opaque barrier ($Z_0 = 2$), a reverse trend is observed. The low bias conductance increases, although the enhance enhancement is small, but noticeable, and a sharp peak is noted at $E \sim \Delta_0$ as shown in Figure 2b.

In equation (21), for a transparent barrier, with increasing RSOC, the contribution of the amplitude of AR (the term coming from a_σ) decreases and the amplitude of NR (the term coming from b_σ) increases. But for an opaque barrier, for the biasing energies, $E < \Delta_0$, the reverse happens, that is the amplitude of NR decreases and the amplitude of AR increases. Thus a scrutiny of Figure 2 yields that RSOC augments the conductance spectrum for $E < \Delta_0$ for a finite opacity ($Z_0 \neq 0$), however the Rashba free case dominates for $E > \Delta_0$, while the latter is always large at all energies for a transparent barrier ($Z_0 = 0$).

Hence we show the variation of the maximum conductance, that is the magnitude of the Andreev peak, G_{max} as a function of Rashba strength, U in Figure 3. It shows the suppression of conductance peak with the increasing strength of RSOC for both the transparent and opaque barriers and the decrease is nearly linear.

Hence we study the conductance characteristics for a d-wave superconductor with $\alpha = 0$ and $\alpha = \pi/4$ (for definition of α, see Fig. 1c). Figures 4a and 4b show the conductance characteristics with $Z_0 = 0$ and $Z_0 = 2$ for $\alpha = 0$. In Figure 4c and 4d we consider $\alpha = \pi/4$ case.

For a d-wave superconductor it is noticed that the conductance decreases with increasing strength of RSOC for transparent barriers ($Z_0 = 0$) for both $\alpha = 0$ and $\alpha = \pi/4$. However for an opaque barrier, we find that for $\alpha = 0$, the low bias conductance increases with RSOC, while for $\alpha = \pi/4$, the same quantity decreases with increasing RSOC. The only exception is observed for the

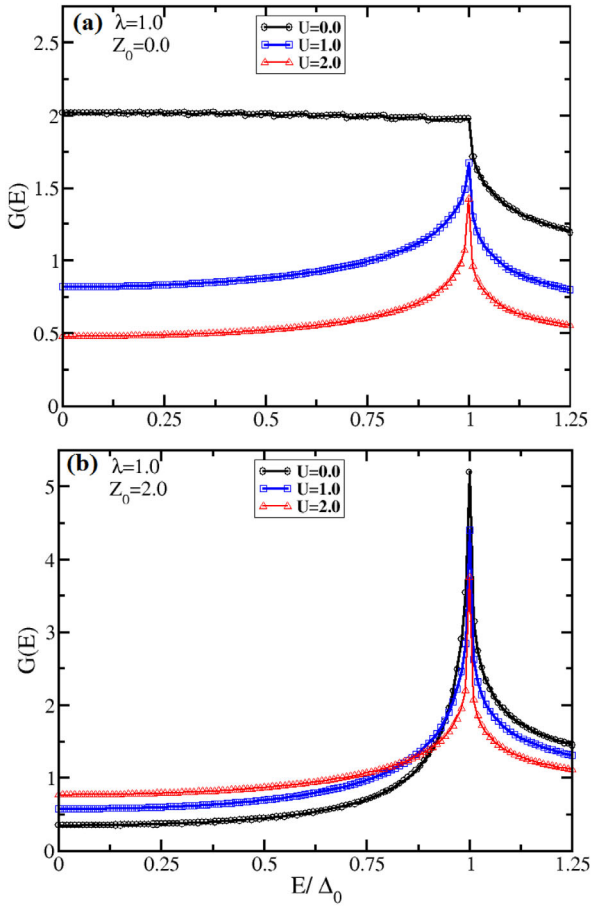

Fig. 2. Black line with circle denotes conductance for $U = 0.0$, the blue line with square denotes conductance for $U = 1.0$ and the red line with triangle denotes conductance for $U = 2.0$. The variation of the conductance, G for a s-wave superconductor as a function of E/Δ_0 for different strengths of RSOC with (a)$Z_0 = 0$, (b) $Z_0 = 2$.

d-wave superconductor with $\alpha = \pi/4$. This is one of the central results of our paper.

For a s-wave superconductor, the crossover between the $U = 0$ and and $U \neq 0$ for opaque barrier case occurs at energies close to Δ_0, while for d-wave the same occurs at $E/\Delta_0 \approx 0.4$.

All of these results have a natural explanation from the behaviour of the AR and NR amplitudes, a_σ and b_σ respectively, which are functions of energy, RSOC, barrier transparency, the asymmetry angle of the d-wave parameter and various other parameters that are going to be discussed in the subsequent sections. Apart from the ratio k^-/k^+ in equation (21), a larger a_σ enhances G_σ, while a larger b_σ decreases it. As we have emphasized earlier, there is no a priori intuition how the interplay of these factors with RSOC in deciding the behaviour of conductance at $E \sim 0$ (that is much less than Δ_0) and $E \sim \Delta_0$.

One may notice an interesting fact that s and d-wave superconductors show dissimilarities in their conductance profile though both have singlet Cooper pairing. For a s-wave superconductor, the electrons with different

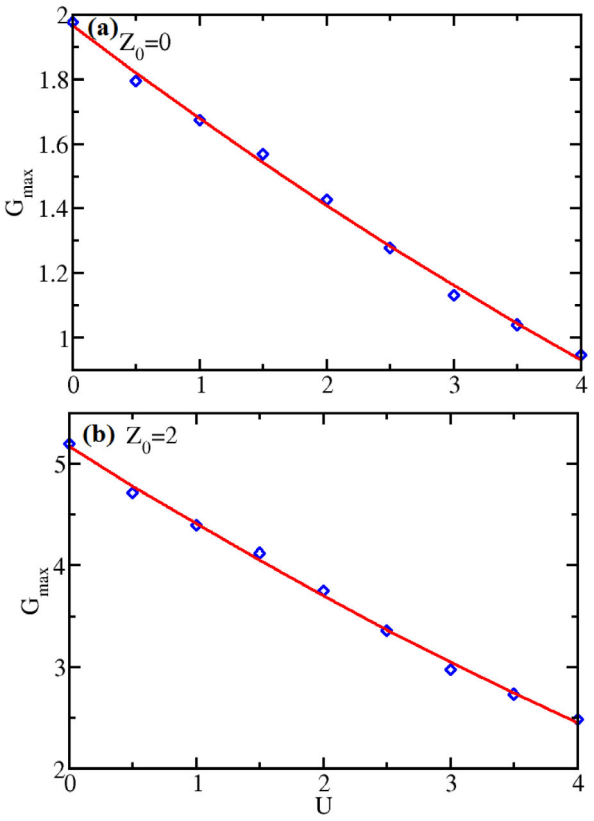

Fig. 3. The variation of the conductance peak, G_{max} for a s-wave superconductor as a function of RSOC strength with (a) $Z_0 = 0$, (b) $Z_0 = 2$.

incident angles are subjected to an isotropic gap in the superconducting region. We find that for all incident angles, the contribution of the AR is maximum with the contribution of the NR being minimum at $E \sim \Delta_0$. So when we integrate the conductance for all incident angles, we get a large value of peak at $E \sim \Delta_0$. But in the case of a d-wave superconductor, the electrons with different incident angles experience different superconducting gaps (see Eq. (6)). So the electrons with different incident angles show maximum contributions at different biasing energies. Therefore the contribution to the conductance coming from different incident angles yield a reduced value for the AR peak at $E = \Delta_0$. Hence the s-wave superconductor has a sharp peak at $E \sim \Delta_0$ while the d-wave shows a moderate peak. The situation is further different for the d-wave superconductor corresponding to $\alpha = \pi/4$. Here we obtain a maximum value at $E = 0$ owing to the fact that the contribution of the AR is maximum at $E = \Delta_0$.

3.1 Finite quasiparticle lifetime

Quasiparticle lifetime, that is the rate at which the quasiparticles decay, especially in disordered superconductors, is an important quantity that characterizes the nature of superconducting state [15]. Recently it was shown the conductivity data of disordered MoC superconducting

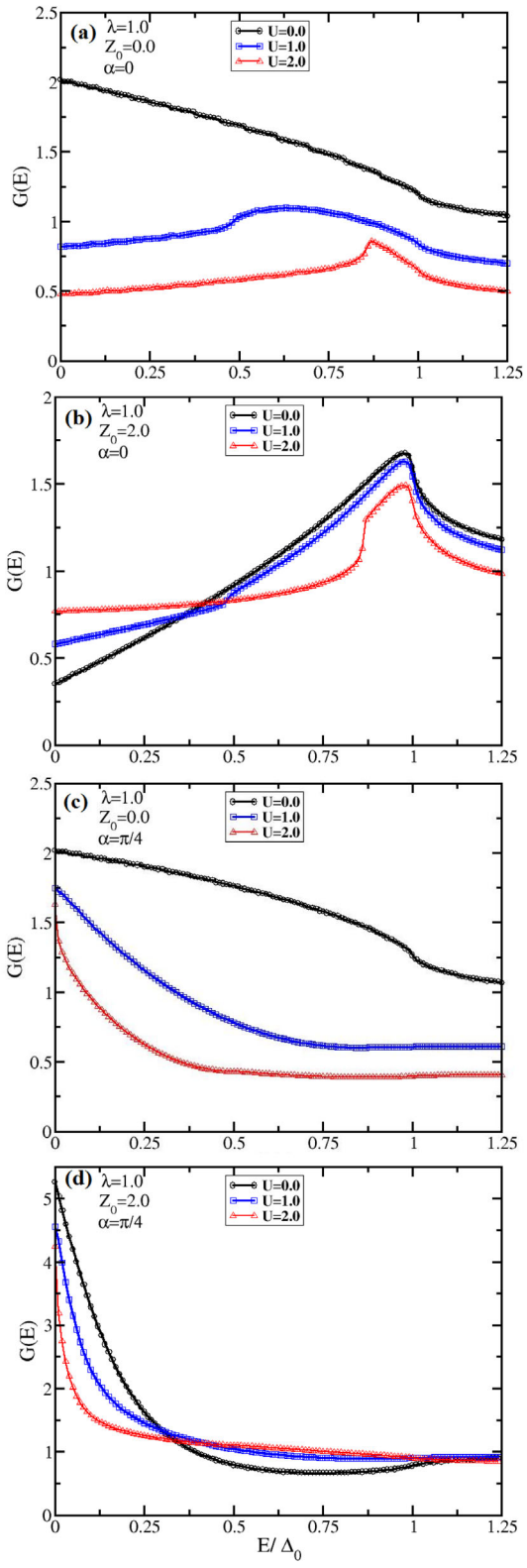

Fig. 4. Black line with circle denotes conductance for $U = 0.0$, the blue line with square denotes conductance for $U = 1.0$ and the red line with triangle denotes conductance for $U = 2.0$. The variation of the conductance, G for a d-wave superconductor as a function of E/Δ_0 for different strengths of RSOC with (a)$Z_0 = 0$ and $\alpha = 0$, (b) $Z_0 = 2$ and $\alpha = 0$, (c) $Z_0 = 0$ and $\alpha = \pi/4$, (d) $Z_0 = 2$ and $\alpha = \pi/4$.

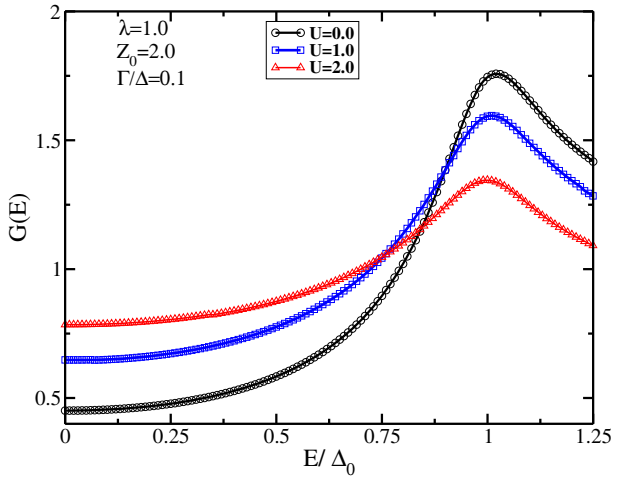

Fig. 5. Black line with circle denotes conductance for $U = 0.0$, the blue line with square denotes conductance for $U = 1.0$ and the red line with triangle denotes conductance for $U = 2.0$. The variation of the conductance, G for a s-wave superconductor as a function of E/Δ_0 for the value of $\Gamma/\Delta = 0.1$.

films [16] can only be satisfactorily explained by invoking a finite quasiparticle lifetime, τ_{QP} denoted by a parameter Γ and defined as,

$$\Gamma \sim \frac{1}{\tau_{QP}} \tag{23}$$

which renormalizes the quasiparticle energies, E by $E \pm i\Gamma$ [17,18]. Without any loss of generality, we have considered only the positive sign in our work.

It should not be a priori evident how an inclusion of Γ (or τ_{QP}) can interfere with the RSOC present in the metallic lead and hence help or hinder the low energy conductance features of a N-S junction. It is nevertheless predictable that a finite Γ would broaden the AR peak and bring down the peak conductance. With the insertion of finite quasiparticle lifetime, all the expressions containing energy, E are renormalized and subsequently they can be plugged to compute the conductance. In Figure 5 we show the variation of G for an opaque barrier ($Z_0 = 2$) for a representative value of $\Gamma/\Delta = 0.1$ for a s-wave superconductor. This value of Γ/Δ_0 is comparable with the value quoted in reference [19] for $CeCoIn_5$ which is a heavy fermion superconductor with a d-wave parameter. In fact various parameters are shown to be, $\Delta_0 = 600\ \mu$eV, $\Gamma = 95\ \mu$eV and Z_{eff} (related to our Z_0)$= 0.28$. The transparent case is an idealized version and hence left out of discussion. A comparison with Figure 2 indicates that finite quasiparticle lifetime affects the conductance peak which broadens and the peak value diminishes.

Hence we study the lifetime effect on tunneling conductance for d-wave superconductor with $\alpha = 0$ and $\pi/4$. Again a finite lifetime broadens and suppresses the conductance profile as noted in Figure 6. The same explanation as detailed earlier at the end of previous subsection holds and not repeated for brevity.

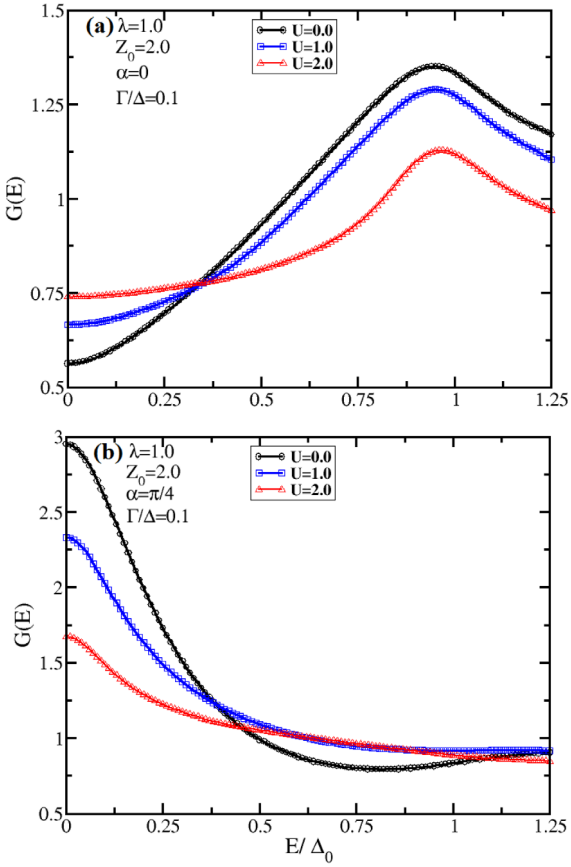

Fig. 6. Black line with circle denotes conductance for $U = 0.0$, the blue line with square denotes conductance for $U = 1.0$ and the red line with triangle denotes conductance for $U = 2.0$. The variation of the conductance, G for a d-wave superconductor as a function of E/Δ_0 for the value of $\Gamma/\Delta = 0.1$ with (a) $\alpha = 0$, (b) $\alpha = \pi/4$.

3.2 Fermi wavevector mismatch

Usually in Andreev reflection across N-S junction experiments, the properties of the Fermi surfaces in both sides of the contact are distinct. Particularly, the Fermi energy in a normal metal depends on the density of the charge carriers present, while the Fermi level dependence enters through the density of states (DOS) at the Fermi energy ($N(E_F)$) in the expression of the transition temperature in conventional superconductors (recalling the BCS expression, $T_c \sim \hbar\omega_D e^{-1/N(E_F)V}$, ω_D being the Debye frequency and V is the interparticle interaction). Thus the Fermi wavevectors appearing in the BTK expression of conductance should naturally be different [20]. However whether and how that affects the conductance characteristics and competes with the RSOC is a topic that needs to be understood. Thus in our work we have considered a parameter λ which denotes the ratio of the Fermi wavevectors in either side of the contact (q_{FS}/k_{FN}) and addressed the interplay of λ and the RSOC on the tunneling studies.

In our work we have kept k_{FN} constant and varied q_{FS}. Thus a competition between two different (namely, RSOC and λ) parameters in the two regions is studied

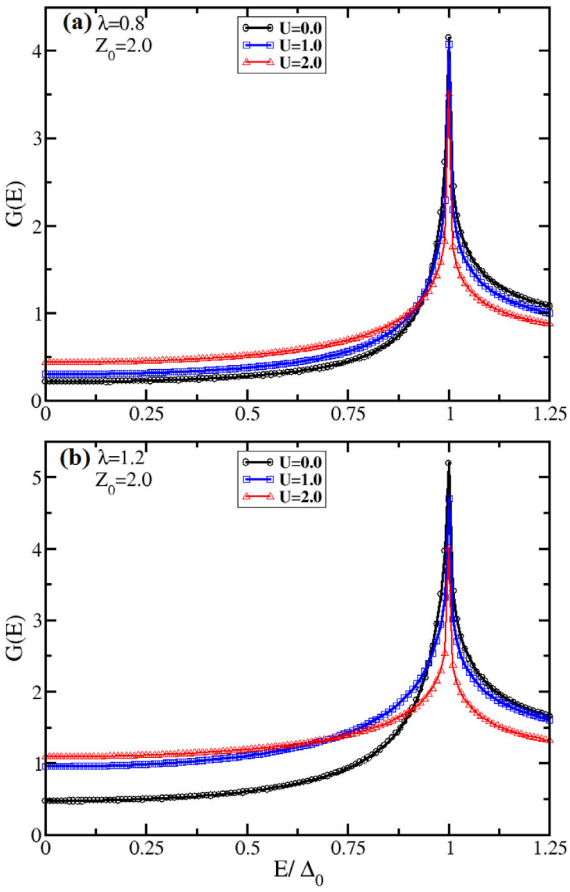

Fig. 7. Black line with circle denotes conductance for $U = 0.0$, the blue line with square denotes conductance for $U = 1.0$ and the red line with triangle denotes conductance for $U = 2.0$. The variation of the conductance, G for a s-wave superconductor as a function of E/Δ_0 for the value of (a) $\lambda = 0.8$, (b) $\lambda = 1.2$.

on the tunneling properties of a junction. We note that the difference between the Fermi wavevectors imposes a constraint on the effective range of angle contributing to the integral in equation (20). For a better understanding, see the discussion at the end of this subsection.

We discuss the case for $\lambda \neq 1$ on the tunneling conductance, in two cases namely, $\lambda = 0.8, 1.2$ for an opaque barrier. Figure 7 shows the variation of $G(E)$ versus E/Δ_0 for a s-wave superconductor. Subsequently the d-wave case is plotted in Figure 8. So considering different wavevector for the carriers in the metallic region and in the superconducting region, we get a similar nature of conductance profile as earlier obtained. The figures for both s and d-wave superconductor reveal that the tunneling conductance enhances with increasing λ for which the effective range of angle contributing to the integral in equation (20) increases causing an enhancement of conductance. For $q_{FS} < k_{FN}$ and for some values of θ_1, the ratio $\frac{k^+}{q^+}$ makes $\sin\theta_{S1} > 1$ which is unphysical. Thus for the above condition, there will not be any transmission to the superconducting region and will not contribute to the conductance. Hence the ratio of the Fermi wavevectors

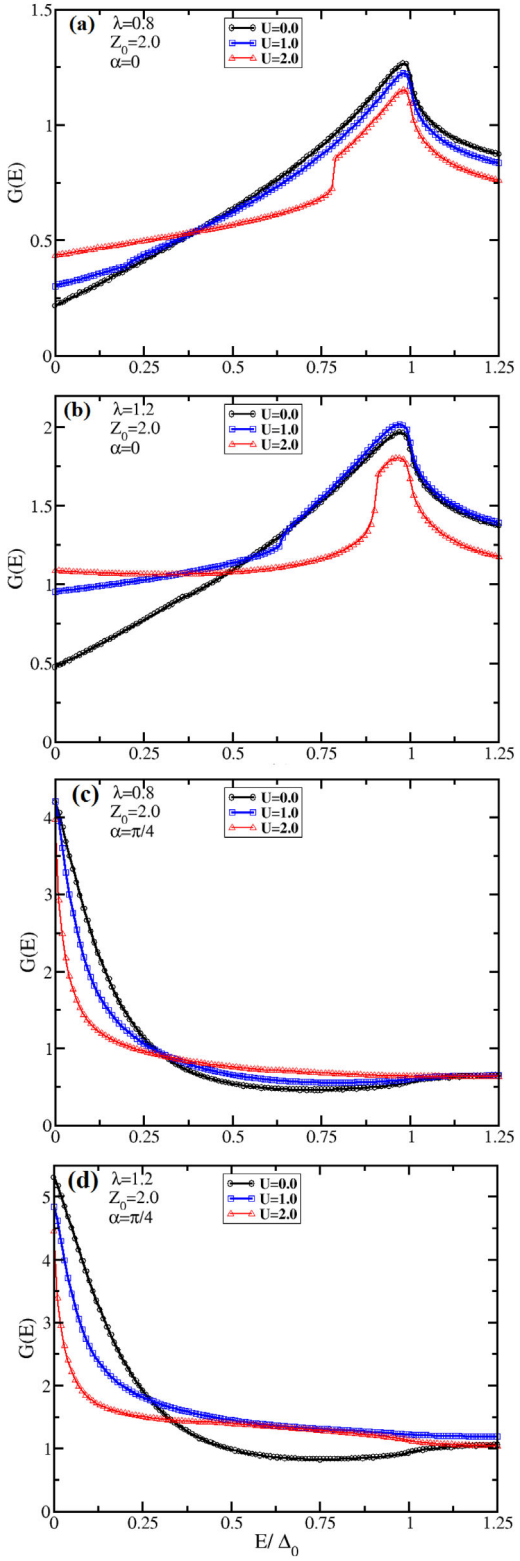

Fig. 8. Black line with circle denotes conductance for $U = 0.0$, the blue line with square denotes conductance for $U = 1.0$ and the red line with triangle denotes conductance for $U = 2.0$. The variation of the conductance, G for a d-wave superconductor as a function of E/Δ_0 for the value of (a) $\lambda = 0.8$ with $\alpha = 0$, (b) $\lambda = 1.2$ with $\alpha = 0$, (c) $\lambda = 0.8$ with $\alpha = \pi/4$, (d) $\lambda = 1.2$ with $\alpha = \pi/4$.

affects the conductance in the following way, for $\lambda > 1$, conductance increases and it diminishes for $\lambda < 1$.

3.3 In-plane magnetic field

The importance of an in-plane magnetic field in the context of a junction device is obvious with the itinerant electrons that exhibit superconductivity below $n \sim 200$ mk at the $LaAlO_3/SrTiO_3$ interface [21,22] is found to have a coexistence with an in-plane polarization of the electronic spins (in-plane magnetization) [23,24]. In fact a large RSOC present at the interface creates an effective spin triplet pairing from singlet superconducting correlations and is also responsible for pairs with finite center of mass momentum, that is the Fulde-Ferrell-Larkin Ovchinnikov (FFLO) state [25]. Emergence of this effective topological superconductivity, starting from a conventional s-wave superconductor raises the possibility of realizing the exotic Majorana physics. Prediction of such a Majorana bound state is done via the presence of a zero mode bound state at the center of the superconducting gap [26].

In our work, to study the effect of an in-plane magnetization on the transmission properties of the N-S junction and the interplay of RSOC therein, we include a parallel magnetic field in the superconducting region. However our study has to be distinguished from the preceding discussion in the following sense. We have not included RSOC in the superconducting leads, and thus there is no relevance to the topological superconductivity that appears above and hence presence of any zero mode state that is protected topologically by the bulk excitation gap is not to be expected. Nevertheless, presence of an in-plane magnetic field (or a magnetization) is still interesting in the context of the junction conductance of a N-S device, if the superconductor is placed in close proximity of a ferromagnet as is done in ferromagnet -superconductor hybrids [27].

In the presence of an in-plane magnetic field, the Hamiltonian in equation (3) gets modified as,

$$H_\sigma = \begin{pmatrix} H_0 + \mu B & \tilde{\Delta} \\ \tilde{\Delta}^\dagger & -H_0 - \mu B \end{pmatrix} \tag{24}$$

where $H_0 = -\frac{\nabla^2}{2} - E_{Fi} + U_\sigma(x)$ and B is strength of in-plane magnetic field ($\mu = 1$ is assumed afterwards). Equation (24) is derived in Appendix B.

With the inclusion of in-plane magnetic field, the momenta of electrons and holes in superconducting region will be modified and are given as,

$$q^+ = q_{FS} + \frac{\sqrt{E^2 - \tilde{\Delta_+}^2} - B}{v_{FS}}$$
$$q^- = q_{FS} - \frac{\sqrt{E^2 - \tilde{\Delta_-}^2} + B}{v_{FS}}. \tag{25}$$

Here we study the variation of conductance, G as the function of E/Δ_0 for a representative value of B, that is $B = 1$ for a s-wave superconductor in Figure 9. The understanding is that the pair breaking effects owing to the inclusion of magnetic field is vanishingly small and thus the superconducting state remains intact in presence of the magnetic field.

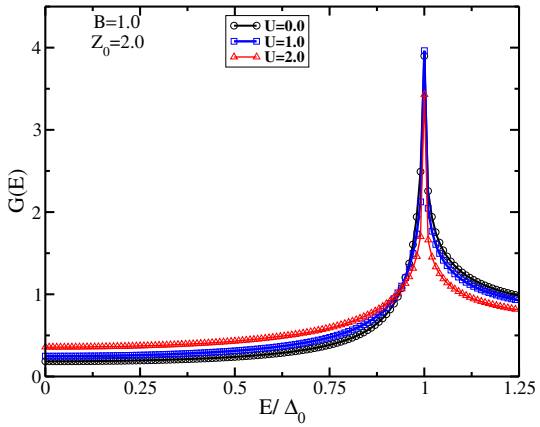

Fig. 9. Black line with circle denotes conductance for $U = 0.0$, the blue line with square denotes conductance for $U = 1.0$ and the red line with triangle denotes conductance for $U = 2.0$. The variation of the conductance, G for a s-wave superconductor as a function of E/Δ_0 for the value of $B = 1$.

Figure 9 shows the suppression of the conductance with the inclusion of the magnetic field where the amplitude of NR (b_σ) is enhanced and the amplitude of AR (a_σ) is found to decrease for $B \neq 0$. Thus from equation (21) it is evident that the presence of an in-plane magnetic field in the superconducting region decreases the tunneling conductance. Apart form this, the magnetic field reduces the effective range of angle contributing to the integral appearing in equation (20) due to the modification of the momenta of electron-like and hole-like quasiparticles as seen from equation (25) (also see Eq. (9)).

Hence we study the magnetic field effect for a d-wave superconductor. Figure 10 contains the variation of conductance, G as the function of E/Δ_0 for an opaque barrier with $\alpha = 0$ and $\pi/4$. Figure 10 also shows the suppression of the tunneling conductance for all values of RSOC.

Probably an in-plane magnetic field is going to have effects on a junction consisting of a normal metal and a superconductor with pairs having finite center of mass momenta.

4 Conclusions

We shall now highlight the key results obtained by us. It is clear that the tunneling conductance is sensitive to the strength of RSOC. For a transparent barrier, RSOC diminishes the conductance for all energies, E in units of Δ_0 for both s and d-wave superconductors. But in the case of a finite opacity, the RSOC enhances the conductance value for biasing energies, $E < \Delta_0$ and suppresses the conductance for $E > \Delta_0$ for a s-wave superconductor. In the d-wave case for finite opacity, this crossover happens for lower value of E compared to the case of s-wave.

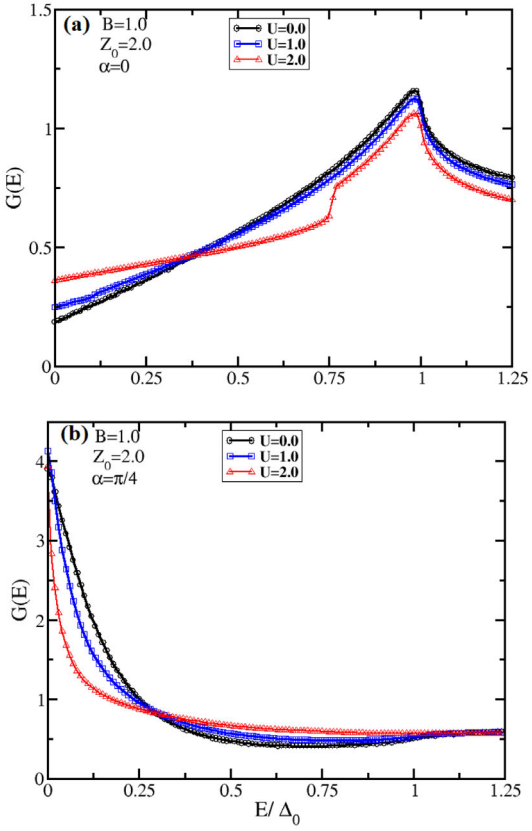

Fig. 10. Black line with circle denotes conductance for $U = 0.0$, the blue line with square denotes conductance for $U = 1.0$ and the red line with triangle denotes conductance for $U = 2.0$. The variation of the conductance, G for a d-wave superconductor as a function of E/Δ_0 for the value of $B = 1$ with (a) $\alpha = 0$, (b) $\alpha = \pi/4$.

Here both $\alpha = 0$ and $\pi/4$ show distinct characters. We find that the the tunneling conductance depends on the quasiparticle lifetime. It broadens the conductance peak and diminishes its value. Further we obtain that the tunneling conductance is getting enhanced with increasing ratio of the Fermi wavevectors (λ). Besides, the inclusion of an in-plane magnetic field shows a significant suppression of tunneling conductance.

We thank SERB, India for financial support under the grant F. No: EMR/2015/001039. Both the authors have contributed equally on the contents of the paper.

Appendix A: Derivation of wavevectors in both sides of the barrier

Here we derive the relationship between the wavevectors in either side of the junction. The Bogoliubov-de Gennes equations are given by,

$$\begin{aligned} H_0 u(r) + \tilde{\Delta} v(r) &= E u(r) \\ -H_0 v(r) + \tilde{\Delta}^\dagger u(r) &= E v(r). \end{aligned} \tag{A.1}$$

When both superconducting gap and potential have slow variation, the Bogoliubov coherence factors can be separated into a rapidly varying part $e^{i\boldsymbol{k}\cdot r}$ with $|\hat{k}| = k_F$ and a slowly varying part. So we can write,

$$u(r) = f(r)e^{ik_F \hat{n}\cdot\boldsymbol{r}} \qquad v(r) = g(r)e^{ik_F \hat{n}\cdot\boldsymbol{r}} \tag{A.2}$$

where $\hat{n}$ is unit vector. Putting equation (A.2) in equation (A.1), and using the facts, $\mu = E_F = v_F^2/2$, $f(r)$ and $g(r)$ are slowly varying on the scale of $1/k_F$ ($\nabla^2 f \ll ik_F \hat{n}\cdot\nabla f$), we get two coupled equations of the form,

$$\begin{aligned} -i\hbar v_f \hat{n}\cdot\hat{\nabla} f(r) + U_\sigma(x) f(r) + \tilde{\Delta} g(r) &= f(r)E \\ i\hbar v_f \hat{n}\cdot\hat{\nabla} g(r) - U_\sigma(x) g(r) + \tilde{\Delta}^\dagger f(r) &= g(r)E. \end{aligned} \tag{A.3}$$

Using the following ansatz $f(r) = f_0 e^{i\tilde{k}\hat{n}\cdot\boldsymbol{r}}$, $g(r) = g_0 e^{i\tilde{k}\hat{n}\cdot\boldsymbol{r}}$, equation (A.3) reduces to,

$$\begin{aligned} \hbar v_f \tilde{k} f_0 - U_\sigma(x) f_0 + \tilde{\Delta} g_0 &= f_0 E \\ -\hbar v_f \tilde{k} g_0 + U_\sigma(x) g_0 + \tilde{\Delta}^\dagger f_0 &= g_0 E. \end{aligned} \tag{A.4}$$

From equation (A.4) we find,

$$\tilde{k}_\pm = \frac{\sigma U k_F \sin\theta_1 \pm \sqrt{E^2 - \tilde{\Delta}^2}}{v_F}. \tag{A.5}$$

The $\pm$ signs refer to the wavevectors for particles and holes. So the momenta expressions for electrons and holes in the normal metal region are,

$$\begin{aligned} k^+ &= k_{FN} + \tilde{k}_+ \\ k^- &= k_{FN} + \tilde{k}_- \end{aligned} \tag{A.6}$$

where k_F is replaced by k_{FN}, v_F is replaced by v_{FN} and $\tilde{\Delta}$ is taken to be zero.

Similarly, the momenta expressions for the electron-like quasiparticles and hole-like quasiparticles in the superconducting region are,

$$\begin{aligned} q^+ &= q_{FS} + \tilde{k}_+ \\ q^- &= q_{FS} + \tilde{k}_- \end{aligned} \tag{A.7}$$

where k_F is replaced by q_{FS}, v_F is replaced by v_{FS} and U is taken as zero (no RSOC is present in the superconducting region).

Appendix B: Derivation of Bogoliubov equations in the presence of in-plane magnetic field

In this appendix we derive the BdG equations in the presence of an in-plane magnetic field. The BCS Hamiltonian is written as,

$$\begin{aligned} H' = &\sum_{i\sigma} c_{i\sigma}^\dagger H_0 c_{i\sigma} + \sum_i \tilde{\Delta}_i c_{i\uparrow}^\dagger c_{i\downarrow}^\dagger \\ &+ \sum_i \tilde{\Delta}_i^\dagger c_{i\uparrow} c_{i\downarrow} + \sum_{i\sigma\sigma'} B(\sigma_x)_{\sigma\sigma'} c_{i\sigma}^\dagger c_{i\sigma'} \end{aligned} \tag{B.1}$$

where $c^{\dagger}_{i\sigma}$ is the creation operator and $c_{i\sigma}$ is the annihilation operator of an electron at the i-th lattice site with spin σ. Considering only first three terms of above equation, the Bogoliubov Valatin transformation gives the BdG equations which can be written in matrix form (see Eq. (3)) in the basis of u_n and v_n.

The transformation can be written as,

$$c_{i\uparrow} = \sum_n [\gamma_{n\uparrow} u_n(i) - \gamma^{\dagger}_{n\downarrow} v^*_n(i)]$$
$$c_{i\downarrow} = \sum_n [\gamma_{n\downarrow} u_n(i) + \gamma^{\dagger}_{n\uparrow} v^*_n(i)] \quad \text{(B.2)}$$

where $\gamma_{n\sigma}$ and $\gamma^{\dagger}_{n\sigma}$ are quasiparticles operators. Those operators must obey the fermion anti-commutation relations,

$$\{\gamma_{m\sigma}, \gamma^{\dagger}_{n\sigma'}\} = \delta_{mn}\delta_{\sigma\sigma'}$$
$$\{\gamma_{m\sigma}, \gamma_{n\sigma'}\} = \{\gamma^{\dagger}_{m\sigma}, \gamma^{\dagger}_{n\sigma'}\} = 0. \quad \text{(B.3)}$$

We wish to make a transformation to a basis such that the Hamiltonian H' is diagonal which will allow us to write,

$$H' = \sum_{n\sigma} \epsilon_n \gamma^{\dagger}_{n\sigma} \gamma_{n\sigma} \quad \text{(B.4)}$$

where ϵ_n is the energy of a quasiparticle excitation for state n. Therefore in the basis in which H' is diagonal we have,

$$[H', \gamma^{\dagger}_{n\sigma}] = \epsilon_n \gamma^{\dagger}_{n\sigma} \quad [H', \gamma_{n\sigma}] = -\epsilon_n \gamma_{n\sigma}. \quad \text{(B.5)}$$

Thus by computing the commutators $[H', c_{m\uparrow}]$ and $[H', c_{m\downarrow}]$ explicitly and comparing coefficients we arrive at the modified BdG equations. Since we know the contribution of first three terms of equation (A.7) in BdG equation, we are now interested only on the last term. The quantities of interest are the commutators,

$$\begin{aligned}[H_B, c_{m\uparrow}] &= -B c_{m\downarrow} \\ &= -B \sum_n [\gamma_{n\downarrow} u_n(m) + \gamma^{\dagger}_{n\uparrow} v^*_n(m)] \\ [H_B, c_{m\downarrow}] &= -B c_{m\uparrow} \\ &= -B \sum_n [\gamma_{n\uparrow} u_n(m) - \gamma^{\dagger}_{n\downarrow} v^*_n(m)] \end{aligned} \quad \text{(B.6)}$$

where $H_B = \sum_{i\sigma\sigma'} B(\sigma_x)_{\sigma\sigma'} c^{\dagger}_{i\sigma} c_{i\sigma'}$. Finally,

$$\begin{aligned}[H', c_{m\uparrow}] &= \sum_n \{[H', \gamma_{n\uparrow}] u_n(m) - [H', \gamma^{\dagger}_{n\downarrow}] v^*_n(m)\} \\ &= -\sum_n \epsilon_n \gamma_{n\uparrow} u_n(m) - \sum_n \epsilon_n \gamma^{\dagger}_{n\downarrow} v^*_n(m) \\ [H', c_{m\downarrow}] &= \sum_n \{[H', \gamma_{n\downarrow}] u_n(m) + [H', \gamma^{\dagger}_{n\uparrow}] v^*_n(m)\} \\ &= -\sum_n \epsilon_n \gamma_{n\downarrow} u_n(m) + \sum_n \epsilon_n \gamma^{\dagger}_{n\uparrow} v^*_n(m). \end{aligned} \quad \text{(B.7)}$$

Comparison of the coefficients of $\gamma_{n\uparrow}$ and $\gamma^{\dagger}_{n\downarrow}$ leads to the following BdG equations,

$$(H_0 + B)u_n + \tilde{\Delta} v_n = \epsilon_n u_n$$
$$\tilde{\Delta}^{\dagger} u_n + (-H_0 - B) v_n = \epsilon_n v_n. \quad \text{(B.8)}$$

These equations are used in Subsection 3.3.

References

1. G. Deutscher, Rev. Mod. Phys. **77**, 109 (2005)
2. D. Daghero, R.S. Gonnelli, Supercond. Sci. Technol. **23**, 043001 (2010)
3. A.F. Andreev, T.M. Rice, Sov. Phys. J. Exp. Theor. Phys. **19**, 1228 (1964)
4. A.F. Andreev, Zh. Eksp. Teor. Fiz **46**, 1823 (1964)
5. A. Furusaki, M. Tsukada, Solid State Commun. **78**, 299 (1991)
6. G.E. Blonder, M. Tinkham, T.M. Klapwijk, Phys. Rev. B **25**, 4515 (1982)
7. P.G. de. Gennes, *Superconductivity of Metals and Alloys* (Westview Press, 1999)
8. T. Matsuyama, R. Kirsten, C. Meiniser, U. Merkt, Phys. Rev. B **61**, 15588 (2000)
9. E.I. Rashba, Fiz. Tverd. Tela **2**, 1224 (1960)
10. J. Nitta, T. Akazaki, H. Takayanagi, T. Enoki, Phys. Rev. Lett. **78**, 1335 (1997)
11. S. Wu, K.V. Samokhin, Phys. Rev. B **81**, 214506 (2010)
12. X. Li, Physica C **485**, 35 (2013)
13. S. Wu, K.V. Samokhin, Phys. Rev. B **82**, 184501 (2010)
14. Z. Yang, J. Wang, K.S. Chan, J. Phys. Soc. Jpn **78**, 084706 (2009)
15. K.E. Gray, J. Phys. F **1**, 290 (1970)
16. M. Zemlicka, P. Neilinger, M. Trgala, M. Rehak, D. Manca, M. Grajcar, Phys. Rev. B **92**, 224506 (2015)
17. A. Plecenik, M. Grajcar, S. Benacka, P. Seidel, A. Pfuch, Phys. Rev. B **49**, 10016 (1994)
18. Y. de Wilde, T.M. Klapwijk, A.G.M. Jansen, J. Heil, P. Wyder, Physica B **218**, 165 (1996)
19. W.K. Park, J.L. Sarrao, J.D. Thompson, L.H. Greene, Phys. Rev. Lett. **100**, 177001 (2008)
20. E. Tuuli, K. Gloos, Low Temp. Phys. **37**, 485 (2011)
21. A. Ohtomo, H.Y. Hwang, Nature **427**, 423 (2004)
22. N. Reyren, S. Thiel, A.D. Caviglia, L. Fitting Kourkoutis, G. Hammerl, C. Richter, C.W. Schneider, T. Kopp, A.-S. Retschi, D. Jaccard, M. Gabay, D.A. Muller, J.-M. Triscone, J. Mannhart, Science **317**, 1196 (2007)
23. L. Li, C. Richter, J. Mannhart, R.C. Ashoori, Nat. Phys. **7**, 762 (2011)
24. J.A. Bert, B. Kalisky, C. Bell, M. Kim, Y. Hikita, H.Y. Hwang, K.A. Moler, Nat. Phys. **7**, 767 (2011)
25. N. Mohanta, A. Taraphder, J. Phys.: Condens. Matter **26**, 025705 (2014)
26. N. Mohanta, A. Taraphder, Europhys. Lett. **108**, 60001 (2014)
27. I.F. Lyuksyutov, V.L. Pokrovsky, Adv. Phys. **54**, 67 (2005)